JMEPEG (2009) 18:255–262
DOI: 10.1007/s11665-008-9277-6
©ASM International
1059-9495/$19.00

Dynamic Contact Performance of Rubber Materials for Designing Wiper Blades

Dazhi Jiang and Dongwei Shu

(Submitted January 15, 2008)

A printer assembly consisting of a pen, wiper with two blades, and wiper blade holder is investigated in this study. The two wiper blades press onto the pen surface via proper dimension interference, while wiping across the pen at a certain speed. A finite element model (FEM) was set up with ANSYS-LSDYNA. The hyper-elastic rubber wiper blades are described by Christensen's model with $n = 1$ for the strain energy density function. Dynamic contact forces between the wiper blades and the pen, number of contacts, and the duration of the wiper blades jumping over the pen are numerically simulated. Effects of the mechanical properties of the rubber materials, i.e., the coefficient of the Christensen's model, C_{10}, on the dynamic contact performance are investigated. The wiper blades are found to periodically touch and jump off from the pen. For the contact between the front blade and the pen, results show that the average contact forces and the number of the contact will increase with C_{10}, and for the back wiper blade there exist the same conclusions, except that the jumping duration of the back wiper blade does not decrease steadily, but shows a minimum. These results suggest that a new design with two curved sides of the blade tip could be beneficence.

Keywords contact force, finite element model, hyper-elastics, rubber materials

1. Introduction

Surface of the pen of a printer is required to be kept clean before printing so that ink can flow smoothly to get a quality print. Rubber wipers are commonly used to remove the dust and residual ink for all kinds of ink printers. Since the rubber materials cover a very wide range of the mechanical properties, i.e., the elastic modulus of the rubber materials may differ by an order of 10^3, the selection of the rubber materials plays an important role for designing a wiper blade.

Rubber (or elastomeric) materials are characterized by very high deformability and essentially complete recoverability after deformation, which is called hyperelastic. There are two efficient approaches to describe the thermo-dynamical behavior of rubber-like solids: the statistical mechanics and the continuum mechanics which are phenomenological. Laraba-Abbesa et al. (Ref 1) have reviewed the existing approaches. In the first approach, the material is described as a macromolecular network structure made of very long and flexible chains (Ref 2, 3). Such macromolecular models are interesting because of their links with a physical reality which provides physical parameters. In the second approach, isotropic hyper-elastic elastomer is conveniently represented in terms of a strain energy density function W (Ref 4-8). Assuming the complete recoverability after deformation, the strain energy density depends only on the final state of strain and in no way on the loading history. Thus, given an undeformed reference state, the state of strain is characterized by the principal stretches λ_1, λ_2, and λ_3 or equivalently by the strain invariants I_1, I_2, and I_3. A rubber can be considered to behave in an incompressible manner as long as the hydrostatic pressures do not become too large. Then, the simplifying assumption of incompressibility is usually adopted, or equivalently the constraint $I_3 = 1$, is identically satisfied throughout the material (Ref 9-14). The basic problem is to construct a strain energy density function, dependent on I_1 and I_2 only, consistent with the observed behavior of rubber-like solids.

LS-Dyna® software is a reliable and robust finite element code and had shown a strong ability to deal with nonlinear problems and large deformation problems in engineering. Christensen's model for hyper-elastic materials (Material Type 77) has been adopted in the materials database of the LS-Dyna® software. In this article, the Christensen's model for hyper-elastic materials is used to describe the strain energy density function, thus the constitutive relation of the rubber materials can be derived based on the strain energy density function. Effects of the properties of rubber materials on dynamic contact forces are investigated by a FEM based on the LS-Dyna®.

2. Constitutive Relationships for Rubber-like Materials

Consider a point initially located at some positions X in a rubber material. Displacement to a new position x after deformation results in a deformation gradient $F = \partial x/\partial X$. Deformation of the material can be described by the left Cauchy-Green deformation tensor $B = (F \cdot \mathrm{F}^T)$, or by the right Cauchy-Green deformation tensor $C = (F^T \cdot \mathrm{F})$, which is related

Dazhi Jiang, Department of Materials Engineering and Applied Chemistry, College of Aerospace and Materials Engineering, National University of Defense Technology, Changsha, Hunan 410073, China; and **Dongwei Shu**, School of Mechanical and Production Engineering, Nanyang Technological University, 50 Nanyang Avenue, Singapore 639798, Singapore. Contact e-mails: mdshu@ntu.edu.sg and jiangdz@nudt.edu.cn.

to the Green strain tensor $E = (C - I)/2$. The three invariants of B are defined by: $I_1 = tr(B)$, $I_2 = [I_1^2 - tr(B^2)]/2$, and $I_3 = det(B)$. It is reasonable to assume that rubber-like materials are incompressible, which results in $I_3 = 1$.

Constitutive relations for an isotropic incompressible hyper-elastic material can be expressed as (Ref 15)

$$\sigma^{e} = -p_e \bar{I} + \alpha_1 \bar{B} + \alpha_2 \bar{B} \cdot \bar{B} \quad \text{(Eq 1)}$$

where p_e is the pressure,

$$\alpha_1 = 2\left(\frac{\partial w}{\partial I_1} + I_1 \frac{\partial w}{\partial I_2}\right)$$
$$\alpha_2 = -2\frac{\partial w}{\partial I_2} \quad \text{(Eq 2)}$$

and σ^e is the Cauchy stress tensor. $w = w(I_1, I_2)$ is a strain energy potential which is assumed to be represented by a polynomial series involving $(I_1 - 3)$ and $(I_2 - 3)$. Brown (Ref 16) has discussed how the number of terms in W affects the resulting stress-strain curves. Based on his analysis and present quasi-static experiments which show that the stress increases rapidly when the strain becomes large, three terms in the polynomial series are sufficient to fit the test data, i.e.,

$$w = A_1(I_1 - 3) + A_2(I_2 - 3) + A_3(I_1 - 3)(I_2 - 3), \quad \text{(Eq 3)}$$

where A_1, A_2, and A_3 are material parameters determined via one-dimensional tests. On the other hand, for the material model of the hyper-elastic rubber adopted in the LS-Dyna®, the energy function w is described as following (Ref 17),

$$w(J_1, J_2, J) = \sum_{p,q=0}^{n} C_{pq}(J_1 - 3)^p (J_2 - 3)^q + w_H(J), \quad \text{(Eq 4)}$$

where $J_1 = I_1 J^{-1/3}$ and $J_2 = I_2 J^{-2/3}$. J is defined as a relative volume, and $J = I_3^{1/2}$. The hydrostatic work term, $w_H(J)$, can be described as (Ref 18)

$$w_H(J) = \frac{1}{2}k(J - 1)^2, \quad \text{(Eq 5)}$$

where k is the bulk modulus of the rubber materials. $w_H(J) = 0$ since the rubber materials are incompressible, which results in $I_3 = 1$ and $J = 1$, and $J_1 = I_1$, $J_2 = I_2$.

Let $n = 1$, Eq 4 can be written as

$$w(I_1, I_2) = C_{10}(I_1 - 3) + C_{01}(I_2 - 3) + C_{11}(I_1 - 3)(I_2 - 3) \quad \text{(Eq 6)}$$

Comparing to Eq 3, one has $A_1 = C_{10}$, $A_2 = C_{01}$, and $A_3 = C_{11}$.

Considering uniaxial loading of a specimen, the stretch in the loading direction is denoted as λ. Hence, the principal stretches are $\lambda_1 = \lambda$, $\lambda_2 = \lambda_3 = \lambda^{-1/2}$. The resulting deformation gradient F and the left Cauchy-Green deformation tensor B (for uniaxial loading, $B = C$) are

$$F = \begin{bmatrix} \lambda & 0 & 0 \\ 0 & \lambda^{-1/2} & 0 \\ 0 & 0 & \lambda^{-1/2} \end{bmatrix}$$
$$B = F \cdot F^{T} = \begin{bmatrix} \lambda^2 & 0 & 0 \\ 0 & \lambda^{-1} & 0 \\ 0 & 0 & \lambda^{-1} \end{bmatrix} \quad \text{(Eq 7)}$$

The invariants are therefore

$$I_1 = tr(B) = \lambda^2 + 2\lambda^{-1}$$
$$I_2 = \frac{1}{2}\left[I_1^2 - tr(B^2)\right] = \lambda^{-2} + 2\lambda \quad \text{(Eq 8)}$$

From Eq 1 and 2, the expression for stress under uniaxial loading is

$$\sigma_{11}^{e} = -p_e + \alpha_1 B_{11} + \alpha_2 B_{11}^2, \quad \text{(Eq 9)}$$

where

$$\alpha_1 = 2\left[C_{10} + C_{01}I_1 + C_{11}\left(I_1^2 - 3I_1 + I_2 - 3\right)\right]$$
$$\alpha_2 = -2[C_{01} + C_{11}(I_1 - 3)] \quad \text{(Eq 10)}$$

and σ_{11}^e is the Cauchy (true) stress. (The engineering stress σ_{11}^0 is related to the true stress by $\sigma_{11}^e = \lambda\sigma_{11}^0$.) The hydrostatic pressure p^e is obtained from the condition $\sigma_{22}^0 = \sigma_{33}^0 = 0$, together with the relation $B_{22} = B_{11}^{-1/2}$:

$$\sigma_{22}^{e} = 0 = -p_e + \alpha_1 B_{11}^{-1/2} + \alpha_2 B_{11}^{-1} \quad \text{(Eq 11)}$$

The constitutive relationship is applied to one-dimensional loading by combining Eq 9 and 10, and this can be written as a function of the stretch λ,

$$\sigma_{11}^{e} = 2\lambda(1 - \lambda^{-3})\{C_{10}\lambda + C_{01} + C_{11}[I_1 - 3 + \lambda(I_2 - 3)]\} \quad \text{(Eq 12)}$$

The relationship between stretch λ and engineering strain ε_{11} in the direction of the uniaxially applied load is $\lambda = 1 + \varepsilon_{11}$. Quasi-static compression tests were conducted on rubber specimens (Ref 19) and Eq 12 was used to fit the experimental data using a simple least-squares approach. Values of the parameters C_{10}, C_{01}, and C_{11} for the rubber materials are $C_{10} = 1.6226$, $C_{01} = -0.4226$, and $C_{11} = 0.0648$. The stress-strain relationships of the rubber materials with different coefficient C_{10} are shown in Fig. 1. As shown in Fig. 1, the

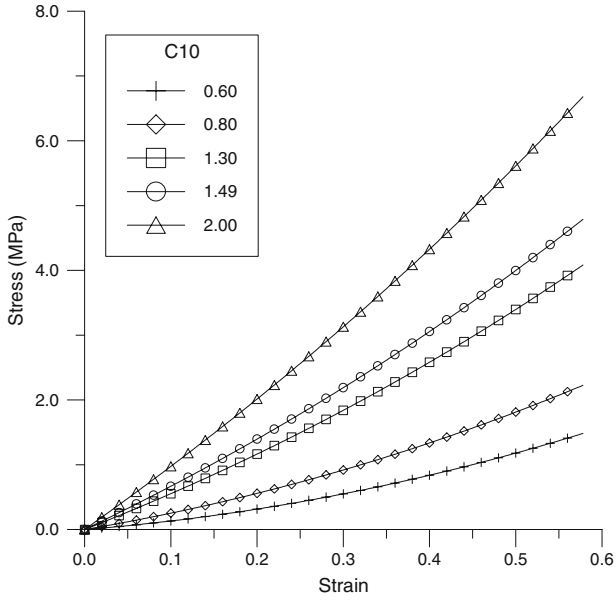

Fig. 1 Simulated stress-strain curves for rubber materials

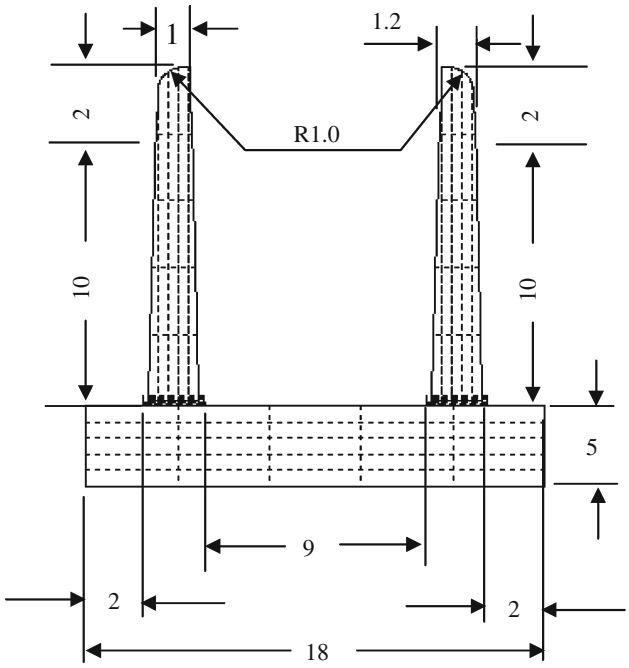

Fig. 2 Dimensions of wiper blades

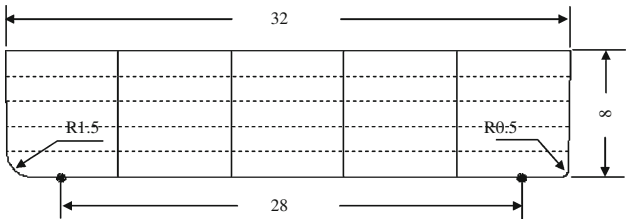

Fig. 3 Dimensions of the pen

initial elastic modulus increases with C_{10}, that means the higher the values of C_{10}, the stiffer the rubber. Meanwhile, the nonlinearity of the stress-strain relations decreases with C_{10}. Our calculation shows that C_{01} and C_{11} have little effects on the stress-strain relations of the rubber materials, and the dynamic performance of the rubber blades. So in the following study, only the effects of C_{10} on properties of the rubber-like materials are considered, with a set of typical values of C_{01} and C_{11} for the rubber.

3. Physical Model

A printer assembly consists of a pen with two encaps at ends, wiper blades, and a wiper blade holder. The assembly is modeled to investigate the effects of the properties of the wiper blades on the dynamical contact performances between the wiper blades and the pen. Dimensions of the printer assembly are shown in Fig. 2 and 3, respectively. Encaps are the names for the two spherical ridges near the two extremes of the pen surface (shown in Fig. 4). The space between the tip of the wiper blades and the pen, A = 1.0 mm, the width of the encap, B = 1.5 mm, and the height of the encap, C = 0.4 mm. The pen and the wiper blade holder are made of steel. The wiper blades are usually made of rubber. For simplicity, the pen and the wiper blade holder are treated as rigid bodies since the elastic modulus of steel is several hundred times that of the rubber. The rubber-like materials used as wiper blades are modeled as incompressible hyper-elastic and can be described by Christensen's model in Eq 12. In the analysis, the pen is fixed and the wiper blades holder moves along Y-axis, as shown in Fig. 4, with a constant velocity of −76.2 mm/s. The Poisson's ratio of the rubber materials is 0.4995 and the density is 1060 kg/m^3. The kinetic coefficient of friction between the wiper blades and the pen is 0.35. The elastic modulus of the pen and the wiper blade

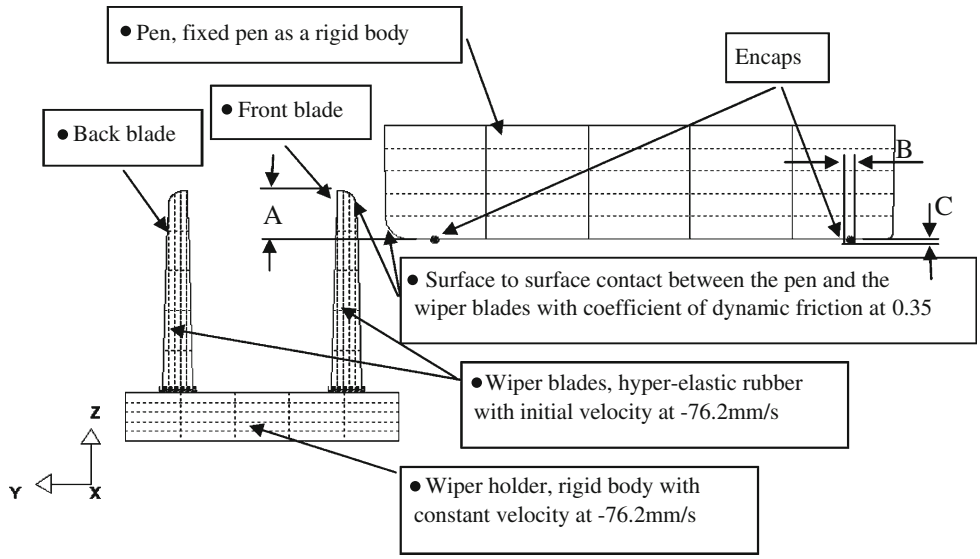

Fig. 4 The physical model of a printer assembly

holder is 210 GPa, Poisson's ratio is 0.25, and density is 7830 kg/m^3.

4. Finite Element Model

The LS-Dyna® finite element program is used to simulate the process of motion between the wiper blades and the pen. To decrease the cost of computation, only a part of the pen and the wiper blade holder are modeled in the finite element simulation since the two parts are considered as rigid bodies. Only one encap is considered due to symmetry. The resultant finite element model is shown in Fig. 5.

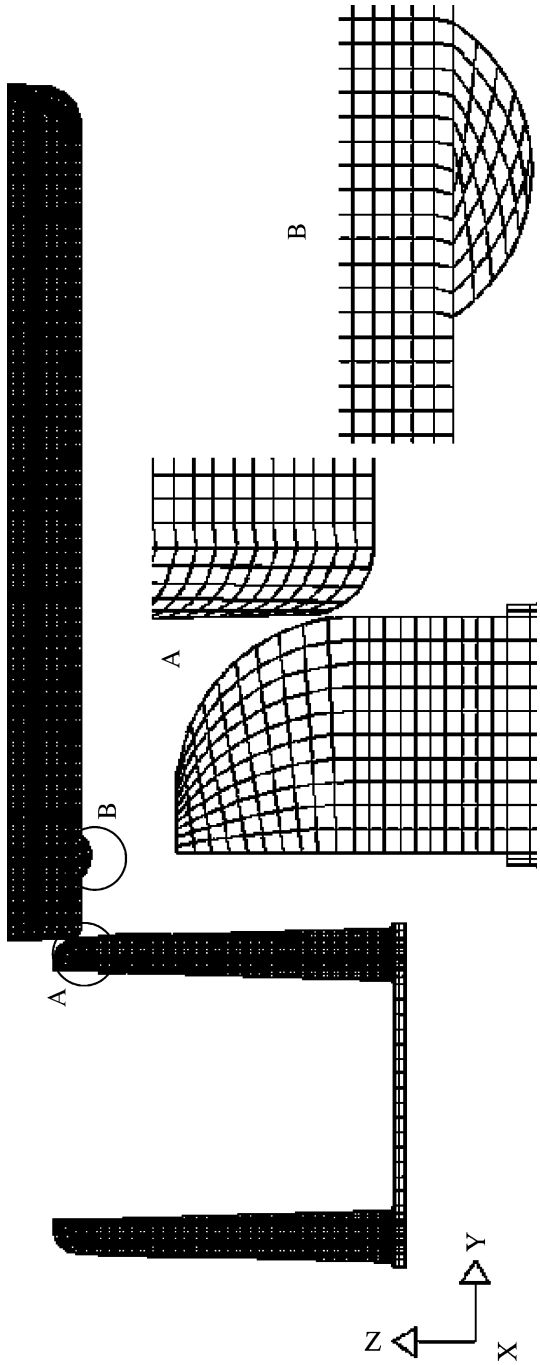

Fig. 5 Finite element model of the printer assembly

5. Results and Discussions

Figure 6(a) shows the contact force on the pen surface (above) and the contact force on the front wiper blade (below), respectively, at C_{10} = 2.0. The curve fitting with polynomials to the order of six gives average values of the contact forces on the wiper blades and the pen, and provides an easier reading of the change of contact forces. Figure 6(b) shows the contact force on the pen surface (above) and on the back wiper blade (below). Several significant stages of the contact can be observed on Fig. 6(a), which shows the contact between wiper blade and pen in stages when the wiper blades move along the surface of the pen. At point *A*, an initial weak collision announces the arrival of the front wiper blade at the pen. At *B*,

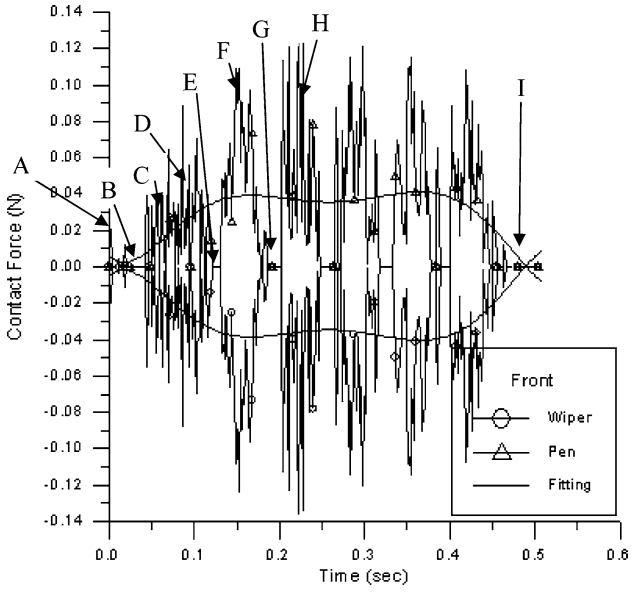

(a) Front wiper blade

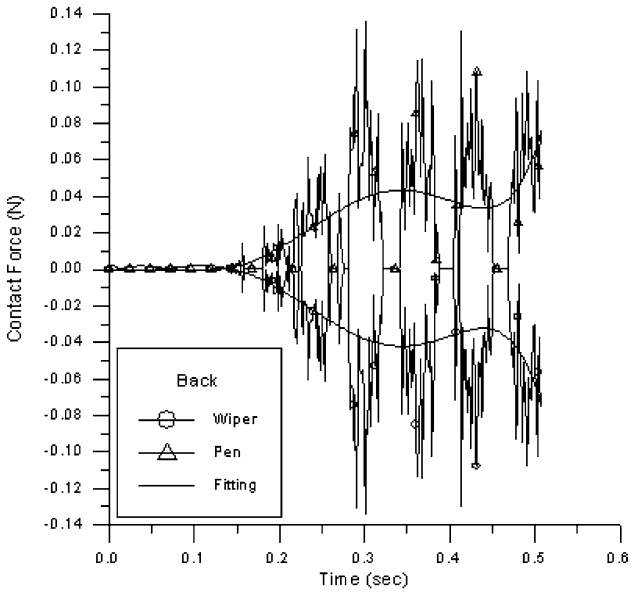

(b) Back wiper blade

Fig. 6 Dynamic contact force on the wiper blades and the pen for C_{10} = 2.00

the weak rebound of the wiper blade after *A*. At *C*, the sharp force increase indicates a second, more severe collision between the blade and the pen, and the rapid climbing of the rubber blade. At *D*, the steady increases of contact force inform us that the blade is nearing the top of the encap. At *E*, the contact forces momentarily fall back to zero, which shows the wiper blade descends to the pen surface after reaching the top of the encap. At *F*, a pulse is produced when the blade collides on the pen again. At *G*, the contact forces again comes back to zero, which shows a jumping (rebound) of the blade off the pen surface after *E* and *F*. The duration corresponding to the zero value of the contact force is defined as *jumping duration* in this article. At *H*, another pulse is produced when the blade collides with the pen again, and after that, the *F*, *G*, and *H* are repeated a few times. The number of these repeated collision and jump off the pen surface of the blade is defined as the *number of contact*. At *I*, the contact forces are finally zero again, which shows the wiper blade moves out of the pen into a free state.

The jumping off the pen by the rubber blades is of interest because at these events, the rubber blade will not wipe the pen surface and the wiping efficiency is low. There is also implication of evenness and thus efficiency of wiping and the time span of the wiper blades. Consequently, the frequency and duration of this event is singled out in this article for further examination.

Figure 6(b) shows contact forces on the back wiper blade and the pen. Basically, the phenomena shown in Fig. 6(b) are similar to that in Fig. 6(a), but happening 0.12 s afterwards, which is the time taken for the encap passing through the distance between the two rubber blades. The average contact forces for the two wiper blades are same, according to the measurement of the fitting curves on Fig. 6(a) and (b), meanwhile the jumping durations for two of them are also almost the same.

Figure 7 shows the contact forces on the front blade, back blade, and the pen, respectively, at C_{10} = 1.49. Compared to the case for C_{10} = 2.0, the average contact force and the number of contacts for the front wiper blade decreases. However, the jumping duration for the front wiper blade increases. For the back wiper blade the average contact force decreases. However, the number of contact remains the same with that in the case for C_{10} = 2.0, and the jumping duration seems to decrease. Compared with C_{10} = 2.0, C_{10} = 1.49 indicates a softer rubber material. This study shows that using a softer material in this

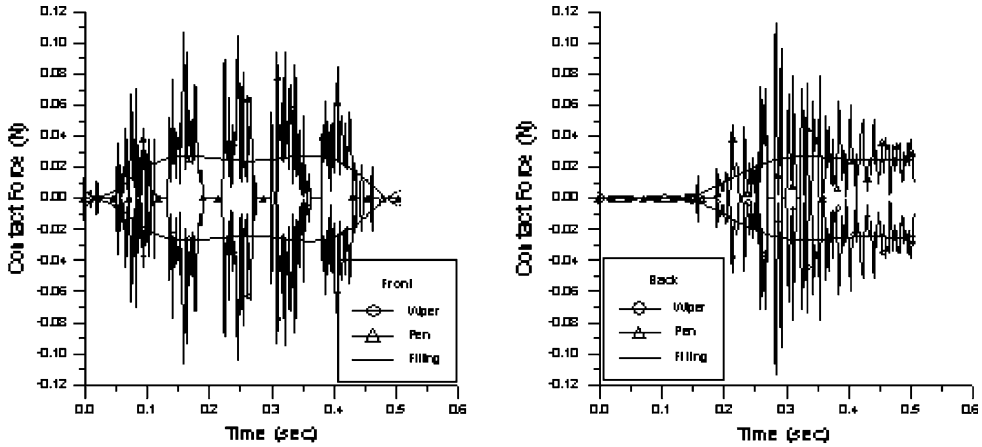

(a) Front wiper blade **(b)** Back wiper blade

Fig. 7 Dynamic contact force on the wiper blades and the pen for C_{10} = 1.49

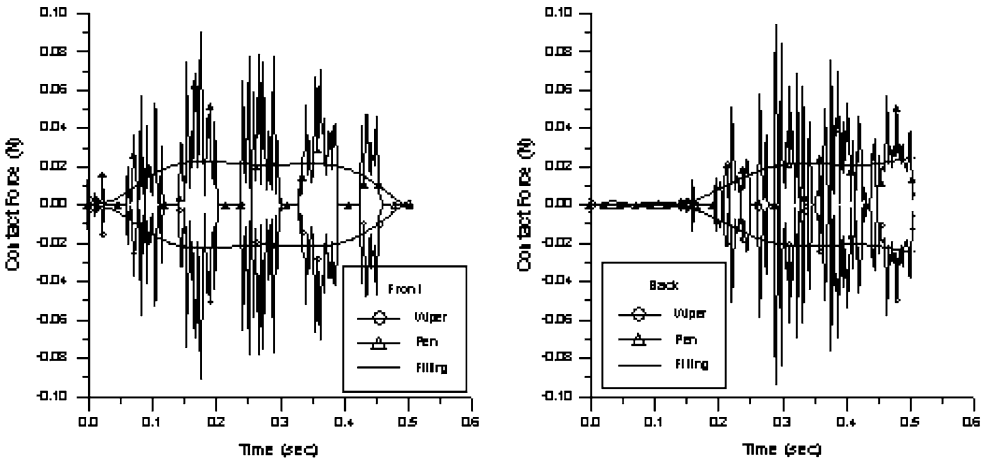

(a) Front wiper blade **(b)** Back wiper blade

Fig. 8 Dynamic contact force on the wiper blades and the pen for C_{10} = 1.30

case reduces contact force but missed a longer distance of wiping as the jumping duration increases. A trade off in design is called for.

Figure 8 shows the contact forces on the wiper blade and the pen, respectively, at $C_{10} = 1.30$. The tendency of the average contact forces, the number of contact, and the jumping duration for the front wiper blade remains the same as that of Fig. 7. However, the back wiper blade in Fig. 8(b) displays some marked changes. The number of contact decreases, compared to Fig. 7(b), while the jumping duration seems to increase. The average contact force, however, appears to remain the same as that of Fig. 7(b).

Figure 9 and 10 shows the contact forces on the wiper blades and the pen at $C_{10} = 0.80$ and $C_{10} = 0.60$, respectively. The tendencies of all performances remain the same compared to the case shown in Fig. 8.

Figure 11 shows the average contact forces on the wiper blades and the pen, respectively, for all cases shown in Fig. 6-10. As shown in Fig. 11, the average contact forces determined by data fitting of the front and back wiper blades are almost same; however, both average contact forces on front and back wiper blades increase with C_{10}. It means that a stiffer rubber may provide the wiper blades tighter contact with the pen. Figure 12 shows the number of contact of the wiper blades when they move along the surface of the pen. The increasing of the number of contact with C_{10} indicates that a stiffer rubber may not move smoothly on the surface of the pen. This dilemma between a tighter contact (good wipe) and smooth wipe (less number of jumps) calls for an optimal value of C_{10}. Figure 13 shows the jumping duration of the wiper blades. The jumping duration of the front wiper blade decreases dramatically with C_{10}; however, the jumping duration of the back wiper blade does not decrease steadily, but shows a minimum. Figure 14 shows the ratio of the jumping duration to wiping duration which is the total duration of the wiper blades contacting the pen. The ratio of the jumping duration for the front wiper blade decreases with C_{10}. It shows again that a stiffer rubber may provide the wiper blades more tight contact with the pen. However, the ratio of the jumping duration for the back wiper blade has a tendency to increase with C_{10}. The result could be due to the shape of the tip of the back wiper blade. Compared to the

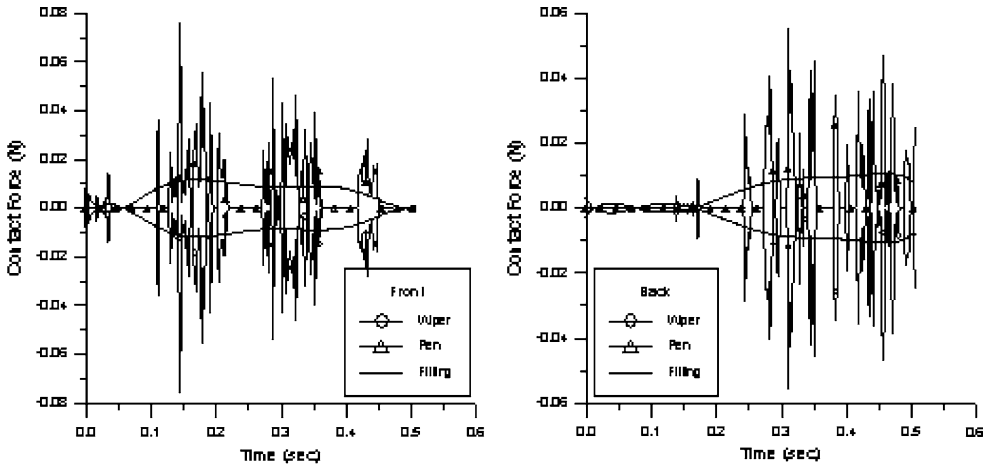

(a) Front wiper blade **(b)** Back wiper blade

Fig. 9 Dynamic contact force on the wiper blades and the pen for $C_{10} = 0.8$

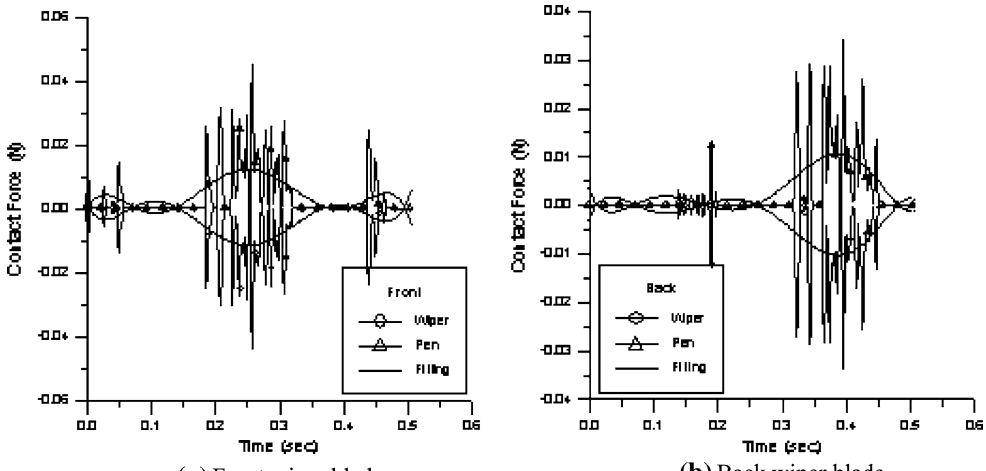

(a) Front wiper blade **(b)** Back wiper blade

Fig. 10 Dynamic contact force on the wiper blades and the pen for $C_{10} = 0.6$

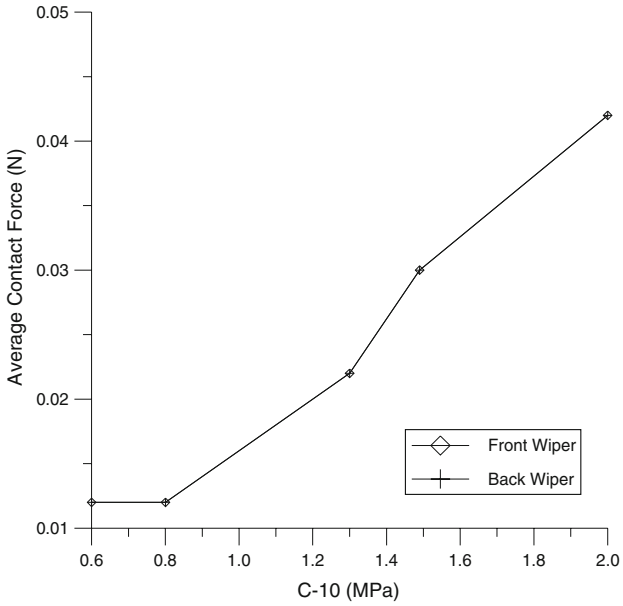

Fig. 11 Average contact forces on wiper blades and pen

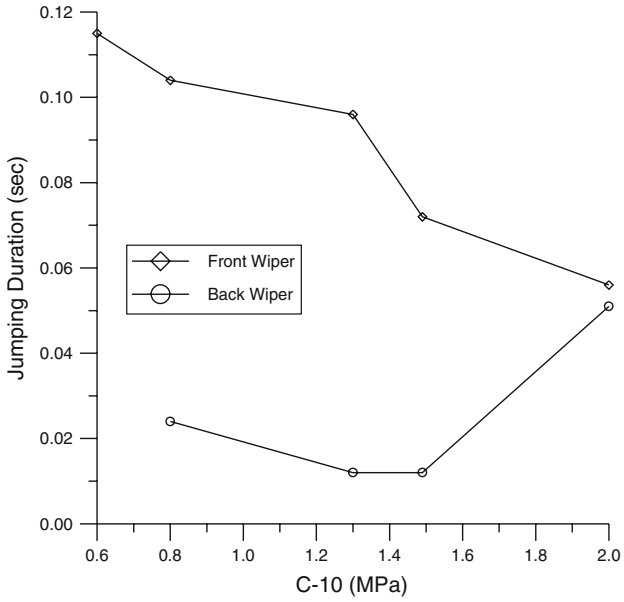

Fig. 13 Jumping duration of wiper blades

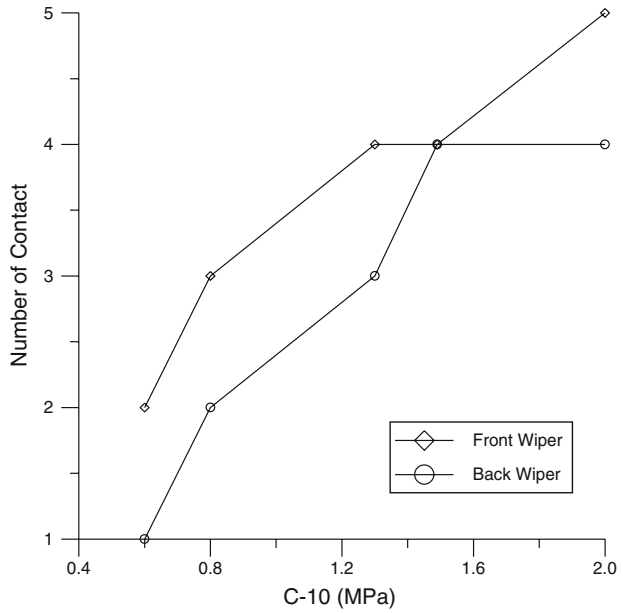

Fig. 12 Number of contact of wiper blades

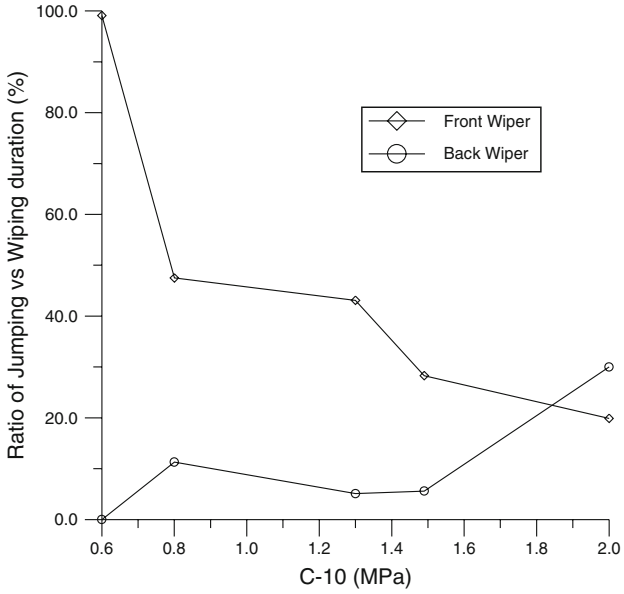

Fig. 14 Ratio of jumping duration to wiping duration

front wiper blade, the contacted side of the tip of the wiper is curved; however, the contacted side of the tip of the back wiper is sharp, therefore the contacted area of the blade with the pen is smaller. Those results show that, for present design of the blades, there is only one wiper blade contacting tightly with the pen in a cycle of motion of the wiper. For forward motion (wiper moves from left side to right side referring to Fig. 4), the wiper blade on the right side (front wiper blade) has a tight contact with the pen. For backward motion (wiper moves from right side to left side referring to Fig. 4), the wiper blade on the left side (back wiper blade) has a tight contact with the pen. To improve the contact conditions of the wiper blades with the pen in either forward or backward motion, a new design with two curved sides of the blade tip could be beneficence.

6. Conclusions

For the front wiper blade, the average contact forces and the number of contact increase with C_{10}, and the jumping duration and the ratio of the jumping duration decreases with C_{10}. For the back wiper blade there exist the same conclusions, except that the jumping duration of the back wiper blade does not decrease steadily, but shows a minimum. To improve the

contact conditions of the wiper blades with the pen in either forward or backward motion, a new design with two curved sides of the blade tip could be beneficence.

References

1. F. Laraba-Abbesa, P. Iennyb, and R. Piques, A New 'Tailor-Made' Methodology for the Mechanical Behaviour Analysis of Rubber-Like Materials: II. Application to the Hyper-Elastic Behaviour Characterization of a Carbon-Black Filled Natural Rubber Vulcanizate, *Polymer*, 2003, **44**, p 821–840
2. J.E. Mark and B. Erman, *A Rubber-Like Elasticity, a Molecular Primer*. Wiley, London, 1987
3. L.R.G. Treloar, *The Physics of Rubber Elasticity*, 3rd ed., Oxford University Press, 1975
4. R.S. Rivlin, Large Elastic Deformations of Isotropic Materials: I. Fundamental Concepts, II. Some Uniqueness Theorems for Pure Homogeneous Deformation, *Philos. Trans. R. Soc. A*, 1948, **240**, p 459–508
5. L.J. Hart-Smith, Elasticity Parameters for Finite Deformations of Rubber-Like Materials, *J. Appl. Math. Phys.*, 1966, **17**, p 608–625
6. H. Alexander, A Constitutive Relation for Rubber-Like Materials, *Int. J. Eng. Sci.*, 1968, **6**, p 549–563
7. R.W. Ogden, Large Deformation Isotropic Elasticity on the Correlation of Theory and Experiment for Incompressible Rubber-Like Solids, *Proc. R. Soc. Lond. A*, 1972, **326**, p 565–584
8. R.M. Christensen, A Nonlinear Theory of Viscoelasticity for Application to Elastomers, *J. Appl. Mech.*, 1980, **47**, p 762–768
9. J.E. Bischoff, E.A. Arrudal, and K. Grosh, A Microstructurally Based Orthotropic Hyper-Elastic Constitutive Law, *J. Appl. Mech.*, 2002, **69**, p 570–579
10. A.F.M.S. Amin, M.S. Alam, and Y. Okui, An Improved Hyper-Elasticity Relation in Modeling Viscoelasticity Response of Natural and High Damping Rubbers in Compression: Experiments, Parameter Identification and Numerical Verification, *Mech. Mater.*, 2002, **34**, p 75–95
11. M.M. Attard, Finite Strain—Isotropic Hyper-Elasticity, *Int. J. Solids Struct.*, 2003, **40**, p 4353–4378
12. T. Beda and Y. Chevalier, Hybrid Continuum Model for Large Elastic Deformation of Rubber, *J. Appl. Phys.*, 2003, **94**(4), p 2701–2706
13. A. Dorfmann and R.W. Ogden, A Pseudo-Elastic Model for Loading, Partial Unloading and Reloading of Particle-Reinforced Rubber, *Int. J. Solids Struct.*, 2003, **40**, p 2699–2714
14. H.J. Qi and M.C. Boyce, Constitutive Model for Stretch-Induced Softening of the Stress-Strain Behavior of Elastomeric Materials, *J. Mech. Phys. Solids*, 2004, **52**, p 2187–2205
15. R.S. Rivlin and D.W. Saunders, Large Elastic Deformations of Isotropic Materials VII. Experiments on the Deformation of Rubber, *Philos. Trans. R. Soc.*, 1951, **243**, p 251–288
16. R.P. Brown, *Physical Testing of Rubber*. 3rd ed., Chapman & Hall, London, 1996
17. LS-Dyna Theoretical Manual, 16.92, 1995
18. T. Sussman and K.J. Bathe, A Finite Element Formulation for Nonlinear Incompressible Elastic and Noninelastic Analysis, *Comput. Struct.*, 1987, **26**, p 357–409
19. L.M. Yang, V.P.W. Shim, and C.T. Lim, A Visco-Hyper-Elastic Approach to Modelling the Constitutive Behaviour of Rubber, *Int. J. Impact Eng.*, 2000, **24**, p 545–560